Open Access

Journal of Energy and Power Technology

LIDSEN Publishing Inc.

Original Research

Nanostructure-Based Solid-State Energy Storage through Hydrogen Trapping in Batteries Using Materials Modelling Technique

Fatemeh Mollaamin *

Department of Biomedical Engineering, Faculty of Engineering and Architecture, Kastamonu University, Kastamonu, Turkey; E-Mail: fmollaamin@kastamonu.edu.tr

* **Correspondence:** Fatemeh Mollaamin; E-Mail: fmollaamin@kastamonu.edu.tr

Academic Editor: Hammad Nazir

Special Issue: Thermal Performance Improvement and Application of Power Batteries

Journal of Energy and Power Technology
2024, volume 6, issue 4
doi:10.21926/jept.2404019

Received: August 15, 2024
Accepted: October 29, 2024
Published: November 07, 2024

Abstract

A comprehensive investigation on hydrogen grabbing by SiO-GeO was carried out, including DFT computations at the CAM-B3LYP-D3/6-311+G (d,p) level of theory. The data shows that if silicon elements are replaced by germanium, the H-grabbing energy will be ameliorated. Electromagnetic and thermodynamic properties of SiO, GeO, and SiO-GeO nanoclusters have been evaluated. The hypothesis of the hydrogen adsorption phenomenon was confirmed by density distributions of PDOS and LOL for hydrated nanoclusters of H-SiO, H-GeO, and H-SiO-GeO-H. The fluctuation in charge density values demonstrates that the electronic densities were mainly located in the boundary of adsorbate/adsorbent atoms during the adsorption status. The advantages of germanium over silicon include its higher electron and hole mobility, allowing germanium devices to operate at higher frequencies than silicon devices. Therefore, by combining SiO and GeO, it can be concluded that the SiO-GeO nanocluster might be an appropriate candidate for hydrogen storage in transistors.

Keywords

Hydrogen adsorption; energy storage; nanocluster; computational method

1. Introduction

A type of clean fuel is hydrogen that might be employed to accumulate, carry, and spread energy produced by other sources, and it generates water when applied in a fuel cell [1]. A fuel cell applies reverse electrolysis to convert an oxidizing agent and hydrogen to power an electric motor [2-4].

CNTs, owing to their lightness, tube construction, vast plane, and high reactivity between C and H atoms, can be proposed as a promising material for H-grabbing [5-12].

It was investigated that H-storing on the C-nano compound indicates molecular hydrogen dissociation [13-16]. The structure of transition metal-carbon exhibits a charge distribution among boundary atoms, and the cationic state of transition metals can be discussed [17-21]. Thus, the electronic charge can be produced through gas molecule adsorption on the surfaces of ionic transition metals [22-24]. Transition metals as dopants might cause a whole Hamiltonian perturbation towards alterations in electronic structures, which converts to substantial usage in magnetic electronic instruments [25-29]. Recently, Si-, Ge- or Sn-carbide nanostructures have been suggested as engaged H-grabbing compounds [30-32]. Since the polarizability of silicon is greater than that of carbon, it is supposed that Si-C/Si nanosheet might attach to compositions more strongly than net carbon nano-surfaces [33-35].

H_2 gas is mostly preserved either by liquefaction under high compressing pressure [36-39] or by adsorption on the surface or interstitial region of the material cavity [40-42]. In relation tTo this, the adsorption of H_2 on the surface of 2D materials has advantages in terms of safe functionality and cost-effectiveness. For the effective utilization of H_2 in fuel cells, the adsorption energy and gravimetric weight percentage on the adsorbent should be sufficiently high [43]. The adsorption-desorption kinetics and the strength of binding energy should be intermediate for hydrogen to bind on the material surfaces with an optimal range of adsorption.

Moreover, the adsorption and sensing of H_2 and CH_2O molecules on the pristine and transition metal consisting of V, Cr, Mn, Nb, Mo, Tc, Ta, W, or Re doping on B or N site of boron nitride nanosheets. The results show that the pristine BNNS indicates fragile interaction with the H_2 and CH_2O molecules. The H_2 and CH_2O molecules might strongly adsorb on the transition metal-doped BNNSs with appreciable adsorption energy through the geometrical deformation on the transition metal doping zone [44].

In our previous works, the investigation of energy storage in fuel cells through hydrogen adsorption has been accomplished using DFT calculations through different nanomaterials consisting of silicon/germanium/tin/lead nano-carbides [45], magnesium -aluminum alloy [46] and aluminum/carbon/silicon doping boron nitride nanocage [47].

Nanomaterials with remarkable specific structures indicate promising applications in energy storage, electrocatalysis, and fuel cells. This article wants to demonstrate a facile approach for fabricating a nanocluster of SiO-GeO as a template at a moderate condition for hydrogen storage. In semiconductor materials, germanium and silicon are essential components that have greatly influenced modern technology. They are vital in electronics, each with distinct properties that make them valuable for different purposes. This article examines the basic difference between germanium and silicon through two complexes of SiO, Ge_5O, and the formation of SiO-GeO nanocluster, including their electrical characteristics and practical uses in different technological fields. One of its notable uses is in the semiconductor industry. Germanium was initially used in early transistors and semiconductors, playing a crucial role in developing electronic devices. However,

silicon largely replaced germanium. Despite this, germanium is still used in niche applications, such as infrared detectors and optical devices.

The present research aims to explore the possibility of using SiO-GeO nanocluster for hydrogen storage by employing first-principles calculations. We have analyzed the structural and electronic properties of SiO, GeO, SiO-GeO, and hydrated nanocluster of H-SiO-GeO-H using state-of-the-art computational techniques.

2. Materials and Methods

This study aims at hydrogen adsorption by using SiO, GeO, and SiO-GeO nanoclusters (Figure 1). The hydrated nanocluster of H-SiO-GeO-H was modeled in the presence of SiO and GeO, and the production of SiO-GeO can increase hydrogen storage in semiconductor transistors. In our research, the calculations were done using the CAM-B3LYP-D3/EPR-3 level of theory.

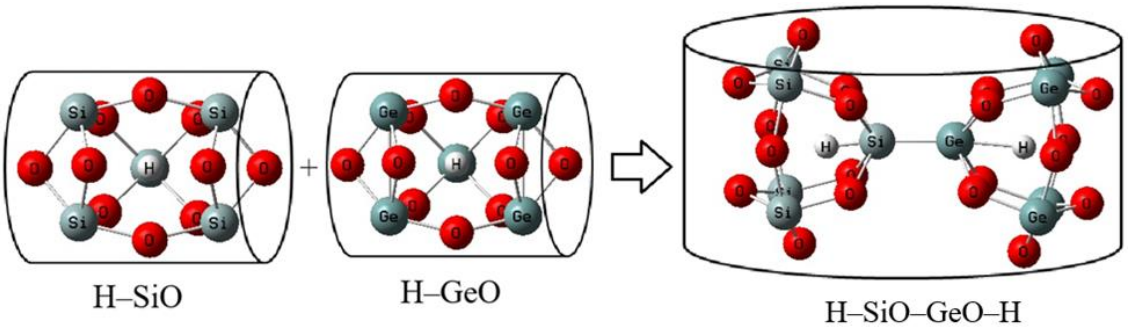

Figure 1 Application of SiO-GeO for increasing hydrogen adsorption towards the energy storage in transistors accompanying formation of hydrated nanoclusters including H-SiO, H-GeO, H-SiO-GeO-H using CAM-B3LYP-D3/6-311+G (d,p) calculation.

Figure 1 shows the process of hydrogen adsorption on the SiO-GeO surface, including the formation of hydrated nanoclusters containing H-SiO, H-GeO, and H-SiO-GeO-H. The Bader charge analysis [48] was discussed during the trapping of hydrogen atoms by Si_5O_{10}-Ge_5O_{10} and the formation of H-SiO, H-GeO, and H-SiO-GeO-H nanoclusters (Figure 1). The rigid potential energy surface using density functional theory [49-62] was performed due to the Gaussian 16 revision C.01 program package [63] and GaussView 6.1 [64]. The coordination input for hydrogen grabbing by SiO-GeO has applied 6-311+G (d,p) and EPR-3 basis sets [65].

3. Results and Discussion

In this article, the data has evaluated the efficiency of boron nitride nanocage doped with chromium, nickel, zinc, molybdenum, palladium, and cadmium for hydrogen detection.

3.1 PDOS Analysis

Squirming the molecular orbital data owing to Gaussian graphs of unit altitude and entire width at half maximum (FWHM) of 0.3 eV by GaussSum 3.0.2 [62] have computed the partial density of states (PDOS) diagrams. To better understand the adsorption characteristics of hydrogen by crystals of SiO and GeO clusters, PDOS has been measured (Figure 2a-d).

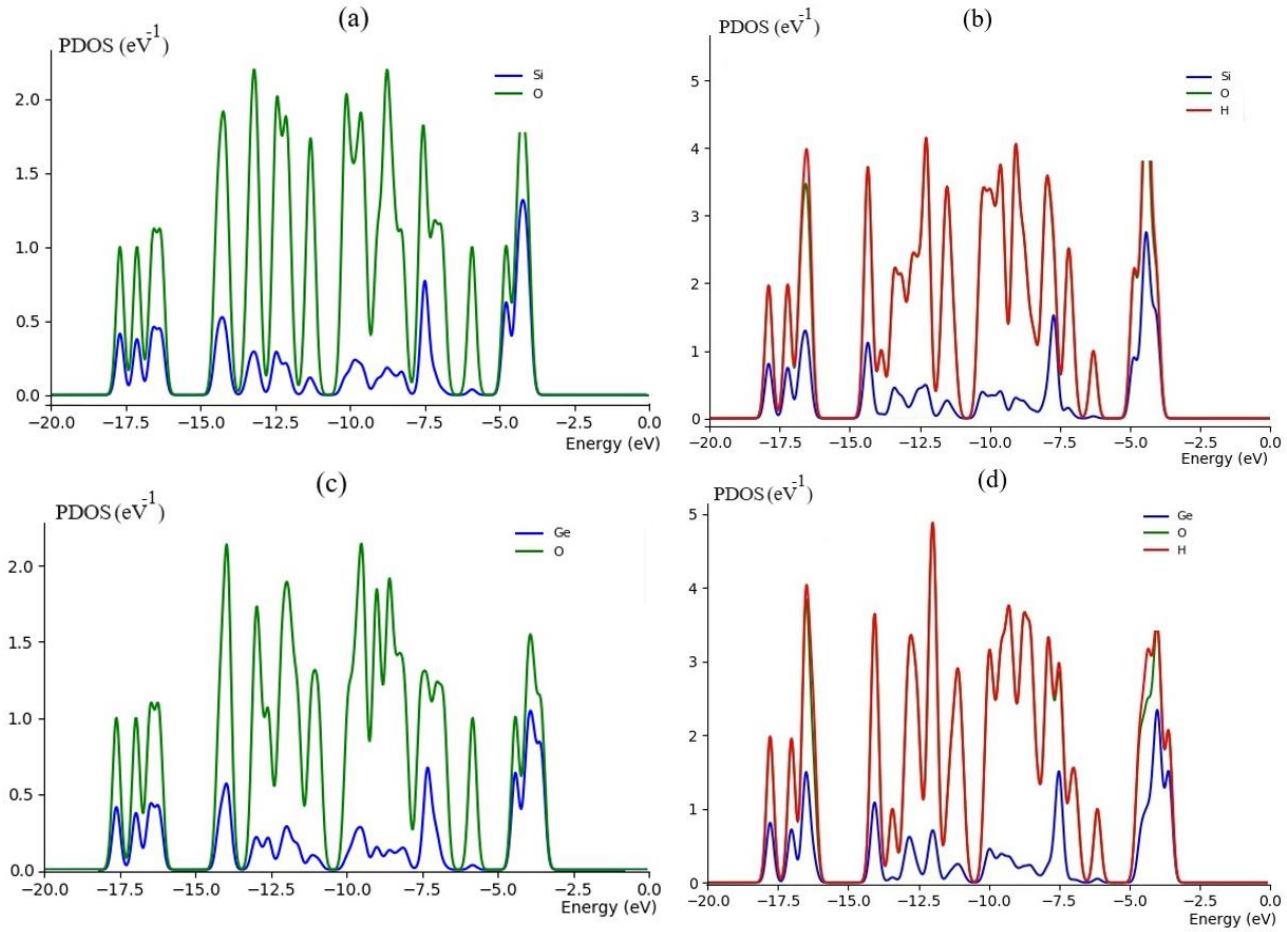

Figure 2 PDOS graphs of (a) SiO, (b) H-SiO, (c) GeO, and (d) H-GeO.

It is clear from the figure that after trapping with hydrogen molecules, p-orbitals of Si and Ge make a significant contribution to the unoccupied level in SiO and GeO. Therefore, the curve of partial PDOS has described the *s* states of H atoms and *p*-orbitals of Si and Ge in the unoccupied level in SiO (Figure 2a) and GeO (Figure 2c) overcome due to the conduction band. A distinguished adsorption trait might be seen in H-SiO and H-GeO because of the potent interaction between the *s* states of hydrogen atoms with *p*-orbitals of Si and Ge in the unoccupied level in SiO and GeO complexes. It has been shown that H-SiO and H-GeO make the most contribution in the middle of the conduction band between -5 to -10 eV. In contrast, the contribution of boron and nitrogen states are enlarged and similar together, and the adsorption of H_2 depicts the interfacial electronic of the SiO and GeO for the selection of hydrogen molecules. H-SiO has indicated sharp peaks for Si atoms close to H atoms in Figure 2b. H-GeO (Figure 2d) has exhibited firm peaks for Ge atoms close to H atoms. Therefore, the order ability of hydrogen adsorption by SiO and GeO based on the PDOS might be shifted as H-GeO > H-SiO.

3.2 LOL Analysis

Localized orbital locator (LOL) has a similar expression compared to the electron localization function (ELF) [66].

$$\mathrm{LOL}(\mathbf{r}) = \frac{\tau(\mathbf{r})}{1+\tau(\mathbf{r})}; \tau(\mathbf{r}) = \frac{D_0(\mathbf{r})}{\frac{1}{2}\sum_i \eta_i \left|\nabla\varphi_i(\mathbf{r})\right|^2} \quad (1)$$

$$D_0(\mathbf{r}) = \frac{3}{10}(6\pi^2)^{2/3}\left[\rho_\alpha(\mathbf{r})^{5/3} + \rho_\beta(\mathbf{r})^{5/3}\right] \quad (2)$$

Multiwfn [67] also supports the approximate version of LOL defined by Tsirelson and Stash [68], namely, the actual kinetic energy term in LOL is replaced by second-order gradient expansion like ELF, which may demonstrate a broad span of bonding samples. This Tsirelson's version of LOL can be activated by setting "ELFLOL_type" to 1. For a special reason, if "ELFLOL_type" in settings.ini is changed from 0 to 2, another formalism will be used:

$$\mathrm{LOL}(\mathbf{r}) = \frac{1}{1+\left[1/\tau(\mathbf{r})\right]^2} \quad (3)$$

If the parameter "ELFLOL_cut" in settings.ini is set to x, then LOL will be zero, where LOL is less than *x*.

The nanoclusters of SiO-GeO and H-SiO-GeO-H can be defined by LOL graphs owing to exploring their delocalization/localization characterizations of electrons and chemical bonds (Figure 3a, 3b). Covalent zones have a high LOL value, and the electron depletion zones between the valence shell and inner shell are indicated by the blue circles around the nuclei (Figure 3a, 3b).

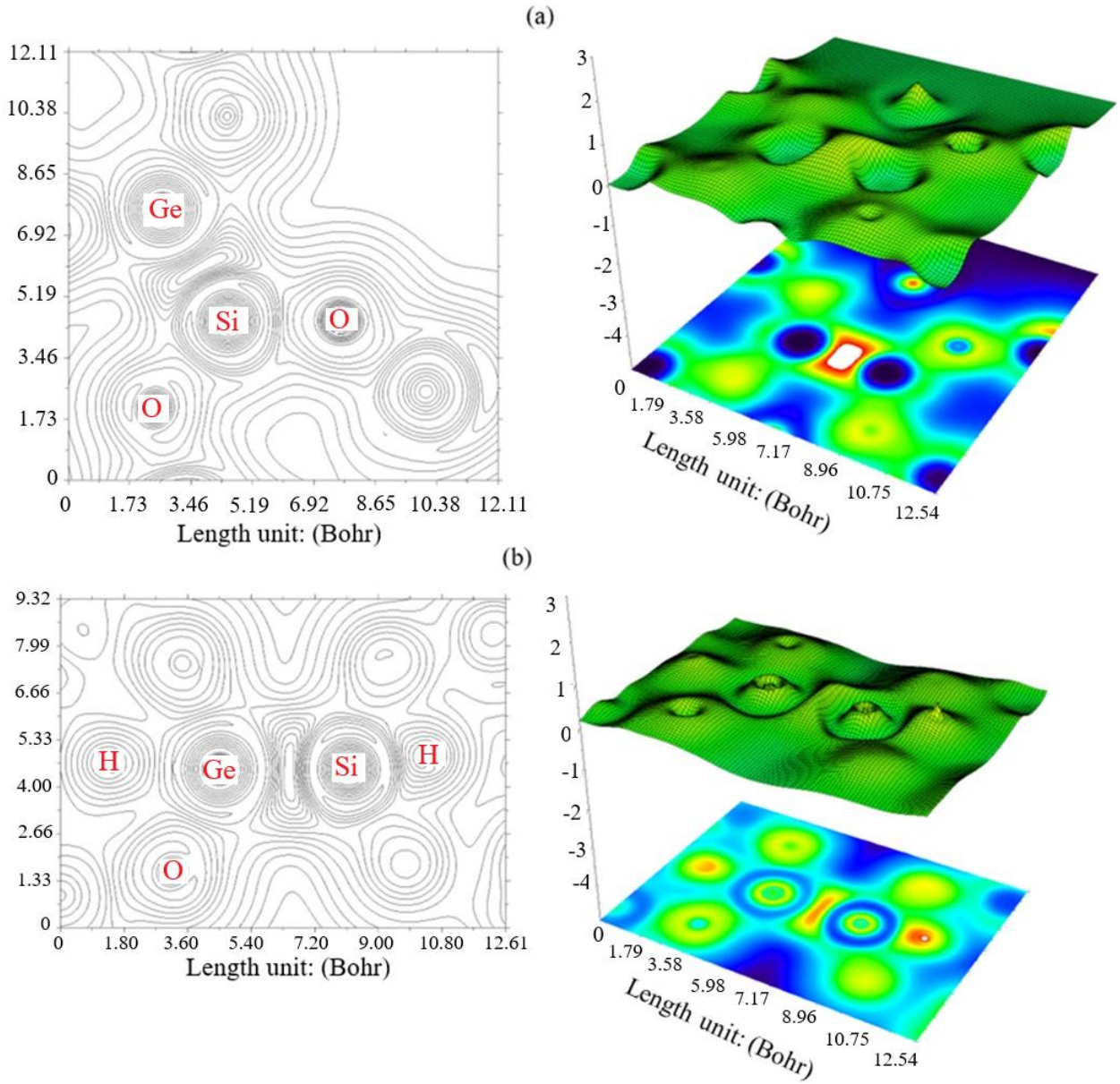

Figure 3 The graphs of LOL for (a) SiO-GeO and (b) H-SiO-GeO-H. (Counter line map on the left and shaded surface map with projection on the right).

The counter map of LOL can confirm that the SiO-GeO (Figure 3a) cluster with labeling atoms of O(10), Si(13), and Ge(28) increases the efficiency during hydrogen adsorption towards the formation of H -SiO-GeO-H (Figure 3b) labeling atoms of Si(13), Ge(28), H(31) or H(32).

3.3 Infrared Spectroscopy, Thermal Performance Promising

The IR has been performed for hydrogen grabbing by SiO and Ge_5O nanoclusters. Therefore, it has been simulated several clusters containing SiO (Figure 4a), H-Si_5O_{10} (Figure 4b), Ge_5O_{10} (Figure 4c), and H-Ge_5O_{10} (Figure 4d).

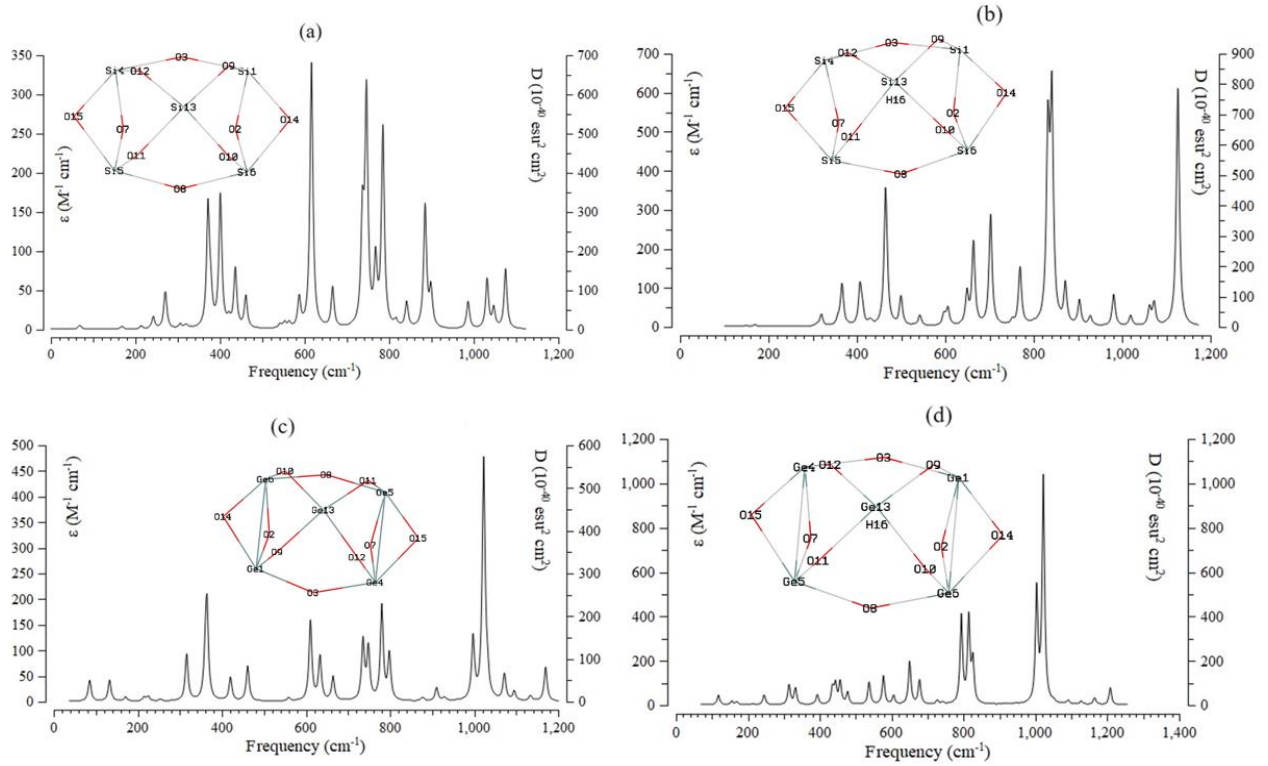

Figure 4 The Frequency (cm^{-1}) changes through the IR spectra for (a) SiO, (b) H-SiO, (c) GeO, and (d) H-GeO complexes.

The frequency values through the IR curves between 200-1100 cm^{-1} have been achieved for Si_5O_{10} with several sharp peaks around 371.52, 400.69, 616.11, 736.73, 746.09, 784.99 and 84.75 cm^{-1} (Figure 4a). Figure 4b shows the frequency range between 300-1200 cm^{-1} for H-Si_5O_{10} with sharp peaks around 464.86, 663.71, 702.49, 832.17, 841.00 and 1126.17 cm^{-1}. Figure 4c indicates the frequency fluctuation between 200-1200 cm^{-1} for Ge_5O_{10} with sharp peaks around 364.39, 610.61, 780.37, and 1022.67 cm^{-1}. The graph of Figure 4d has been observed in the frequency range between 200-1200 cm^{-1} for H-Ge_5O_{10}, with several sharp peaks around 793.72, 814.41, 1003.50, and 1021.96 cm^{-1}. Hydrogen capture with Si_5O_{10} and Ge_5O_{10} nanoclusters has described that the frame of the overcoming cluster is related to Ge_5O_{10} in the high amounts of frequency. This property makes germanium potentially advantageous for specific high-frequency applications requiring faster transistor switching speeds. The advantages of germanium over silicon include its higher electron and hole mobility, allowing it to operate at higher frequencies than silicon devices.

Table 1, through the thermodynamic specifications at 298 K, concluded that the Si_5O_{10}-Ge_5O_{10} nanocluster might be a more efficient structure for hydrogen trapping.

Table 1 The thermodynamic characters of SiO, H-SiO, GeO, H-GeO, Si_5O_{10}-Ge_5O_{10} and H-SiO-GeO-H nanoclusters using CAM-B3LYP-D3/6-311+G (d,p) calculation.

Compound	$\Delta E^o_{ads} \times 10^{-3}$ (kcal/mol)	$\Delta H^o_{ads} \times 10^{-3}$ (kcal/mol)	$\Delta G^o_{ads} \times 10^{-3}$ (kcal/mol)	Dipole moment (Debye)
SiO	-1379.64	-1379.64	-1379.64	0.44
H-SiO	-1379.93	-1379.93	-1379.96	0.73
GeO	-6981.16	-6981.16	-6981.20	0.80
H-GeO	-6981.44	-6981.44	-6981.47	0.59
SiO-GeO	-8360.86	-8360.86	-8360.89	1.27
H-SiO-GeO-H	-8361.37	-8361.37	-8361.39	1.54

Thermodynamic parameters of hydrogen adsorption on SiO, GeO, and SiO-GeO nanoclusters have been assigned through a given number of hydrogen donor sites. The stabilities of the linkage of two complexes of SiO, GeO, and the formation of SiO-GeO nanocluster can be considered as H-SiO-Ge_5O-H > SiO-GeO > H-GeO > GeO > H-SiO > SiO complexes (Table 1).

The changes of Gibbs free energy versus dipole moment could detect the maximum efficiency of SiO-GeO for hydrogen adsorption through ΔG^o_{ads} which is related to the linkage between hydrogen atoms with silicon and germanium in SiO-GeO and the formation of hydrated nanocluster of H-SiO-GeO-H.

The adsorption process of hydrogen atoms on SiO, GeO, and SiO-GeO nanoclusters is affirmed by the ΔG^o_{ads} quantities:

$$\Delta G^o_{ads} = \Delta G^o_{H-SiO-GeO-H} - (\Delta G^o_{SiO} + \Delta G^o_{H-SiO} + \Delta G^o_{GeO} + \Delta G^o_{H-GeO}) \quad (4)$$

Table 1 shows the key role of interaction between the adsorbate of hydrogen atoms as the electron donors and the adsorbent of SiO, GeO and SiO-GeO nanocluster as the electron acceptors. As a result, germanium has interesting optical properties, including transparency to infrared radiation. This characteristic makes it valuable in the production of lenses for thermal imaging systems and night vision devices. Its use extends to fiber optics, where it serves as a dopant to enhance the refractive index of optical fibers, improving signal transmission. Therefore, combining SiO and GeO and producing a SiO-GeO nanocluster can promise enhancing hydrogen storage in the transistors by forming the hydrated cluster of H-SiO-GeO-H.

Then, current numerical simulations and theoretical research on the heat transfer limit of HTHPs are recommended. The significant hypotheses in numerical simulations and the present theoretical studies are compiled here. Finally, some potential future directions and tentative suggestions for HTHP research are put forward.

Furthermore, this design can improve the performance of automotive battery thermal management systems to accomplish more effective heat dissipation. The thermochemistry parameters and characteristics of composite thermally conductive silicone-germanium materials of SiO, GeO and SiO-GeO are recommended. The remarkable hypotheses applied in numerical simulations and the present theoretical investigation are assembled in this work. Therefore, it is a considerable viewpoint of the optimal operating conditions for each direction, and it is expected this paper contribute to improving the thermal performance of batteries.

4. Conclusion

In summary, H-grabbing on the nanoclusters of SiO, GeO, and SiO-GeO was investigated by first-principle calculations. The alterations of charge density illustrated a remarkable charge transfer towards SiO, GeO, and SiO-GeO, which might play the electron acceptor roles. At the same time, H-atoms act as the stronger electron donner through adsorption on the SiO, GeO, and SiO-GeO. SiO, GeO, and SiO-GeO have greater interaction energy from Van der Waals' forces with H-atoms, which can cause them to be much more resistant. Besides, thermodynamic parameters describing H-grabbing on the nano-carbides of SiO, GeO and SiO-GeO have been investigated, including the internal process of the adsorbent-adsorbate system. As germanium has shown interesting optical properties, including transparency to infrared radiation, a combination of Si_5O_{10} and GeO and producing SiO-GeO nanocluster can promise to enhance hydrogen storage in the transistors through the formation of the hydrated cluster of H-SiO-GeO-H. Thermodynamic parameters have constructed a detailed molecular model for atom-atom interactions and a distribution of point charges, which can reproduce the polarity of the solid material and the adsorbing molecules. Today, it is crucial to distinguish the potential of hydrogen technologies and bring up all perspectives of their performance, from technological progress to economic and social effects. The authors intend to pursue research on sustainability and clean energy subjects to find new solutions for reducing the global dependency on fossil fuels.

Author Contributions

Fatemeh Mollaamin (F.M.): Conceptualization, writing – original draft, formal analysis, writing – review and editing. The author has read and approved the published version of the manuscript.

Competing Interests

The authors have declared that no competing interests exist.

References

1. Reza MS, Mannan M, Wali SB, Hannan MA, Jern KP, Rahman SA, et al. Energy storage integration towards achieving grid decarbonization: A bibliometric analysis and future directions. J Energy Storage. 2021; 41: 102855.
2. Olabi AG, Sayed ET. Developments in hydrogen fuel cells. Energies. 2023; 16: 2431.
3. Monajjemi M, Baei MT, Mollaamin F. Quantum mechanic study of hydrogen chemisorptions on nanocluster vanadium surface. Russ J Inorg Chem. 2008; 53: 1430–1437.
4. Das V, Padmanaban S, Venkitusamy K, Selvamuthukumaran R, Blaabjerg F, Siano P. Recent advances and challenges of fuel cell based power system architectures and control-a review. Renew Sustain Energy Rev. 2017; 73: 10-18.
5. Lobo R, Ribeiro J, Inok F. Hydrogen uptake and release in carbon nanotube electrocatalysts. Nanomaterials. 2021; 11: 975.
6. Feng X, Sun L, Wang W, Zhao Y, Shi JW. Construction of CdS@ZnO core-shell nanorod arrays by atomic layer deposition for efficient photoelectrochemical H_2 evolution. Sep Purif Technol. 2023; 324: 124520.

7. Ströbel R, Garche J, Moseley PT, Jörissen L, Wolf G. Hydrogen storage by carbon materials. J Power Sources. 2006; 159: 781-801.
8. Baughman RH, Zakhidov AA, De Heer WA. Carbon nanotubes-the route toward applications. Science. 2002; 297: 787-792.
9. Azad UP, Chandra P. Handbook of nanobioelectrochemistry: Application in devices and biomolecular sensing. Singapore: Springer; 2023.
10. Kumar A, Purohit B, Mahato K, Roy S, Srivastava A, Chandra P. Design and development of ultrafast sinapic acid sensor based on electrochemically nanotuned gold nanoparticles and solvothermally reduced graphene oxide. Electroanalysis. 2020; 32: 59-69.
11. Kadian S, Arya BD, Kumar S, Sharma SN, Chauhan RP, Srivastava A, et al. Synthesis and application of PHT-TiO_2 nanohybrid for amperometric glucose detection in human saliva sample. Electroanalysis. 2018; 30: 2793-2802.
12. Kumari R, Mendki N, Chandra P. Smartphone-integrated automated sensor employing electrochemically engineered 3D bimetallic nanoflowers for hydrogen peroxide quantification in milk. Langmuir. 2024; 40: 11146-11159.
13. Yang CM, Kanoh H, Kaneko K, Yudasaka M, Iijima S. Adsorption behaviors of HiPco single-walled carbon nanotube aggregates for alcohol vapors. J Phys Chem B. 2002; 106: 8994-8999.
14. Zhao Y, Kim YH, Dillon AC, Heben MJ, Zhang SB. Ab initio design of Ca-decorated organic frameworks for high capacity molecular hydrogen storage with enhanced binding. Phys Rev Lett. 2005; 94: 155504.
15. Back CK, Sandí G, Prakash J, Hranisavljevic J. Hydrogen sorption on palladium-doped sepiolite-derived carbon nanofibers. J Phys Chem B. 2006; 110: 16225-16231.
16. Novoselov KS, Geim AK, Morozov SV, Jiang DE, Zhang Y, Dubonos SV, et al. Electric field effect in atomically thin carbon films. Science. 2004; 306: 666-669.
17. Geim AK. Graphene: Status and prospects. Science. 2009; 324: 1530-1534.
18. Castro Neto AH, Guinea F, Peres NM, Novoselov KS, Geim AK. The electronic properties of graphene. Rev Mod Phys. 2009; 81: 109-162.
19. Mak KF, Lee C, Hone J, Shan J, Heinz TF. Atomically thin MoS_2: A new direct-gap semiconductor. Phys Rev Lett. 2010; 105: 136805-136807.
20. Radisavljevic B, Radenovic A, Brivio J, Giacometti V, Kis A. Single-layer MoS_2 transistors. Nat Nanotechnol. 2011; 6: 147-150.
21. Rodin AS, Carvalho A, Castro Neto AH. Strain-induced gap modification in black phosphorus. Phys Rev Lett. 2014; 112: 176801-176803.
22. Mollaamin F, Monajjemi M. Trapping of toxic heavy metals from water by GN-nanocage: Application of nanomaterials for contaminant removal technique. J Mol Struct. 2024; 1300: 137214.
23. Fei R, Faghaninia A, Soklaski R, Yan JA, Lo C, Yang L. Enhanced thermoelectric efficiency via orthogonal electrical and thermal conductances in phosphorene. Nano Lett. 2014; 14: 6393-6399.
24. Ramasubramaniam A, Muniz AR. Ab initio studies of thermodynamic and electronic properties of phosphorene nanoribbons. Phys Rev B. 2014; 90: 085424-085429.
25. Yan Z, Bai Y, Sun L. Adsorption of thiophene and SO_x molecules on Cr-doped and Ti-doped graphene nanosheets: A DFT study. Mater Res Express. 2019; 6: 125067.

26. Mollaamin F, Monajjemi M. In situ Ti-embedded SiC as chemiresistive nanosensor for safety monitoring of CO, CO_2, NO, NO_2: Molecular modelling by conceptual density functional theory. J Phys Chem B. 2024; 18: 49-66.
27. Mollaamin F, Monajjemi M. Application of DFT and TD-DFT on Langmuir Adsorption of Nitrogen and Sulfur Heterocycle Dopants on an Aluminum Surface Decorated with Magnesium and Silicon. Computation. 2023; 11: 108.
28. Javan MB. Electronic and magnetic properties of monolayer SiC sheet doped with 3d-transition metals. J Magn Magn Mater. 2016; 401: 656-661.
29. Wu Y, Zhou L, Du X, Yang Y. Near-field radiative heat transfer between two SiC plates with/without coated metal films. J Nanosci Nanotechnol. 2015; 15: 3017-3024.
30. Nazeer W, Farooq A, Younas M, Munir M, Kang SM. On molecular descriptors of carbon nanocones. Biomolecules. 2018; 8: 92.
31. Zhao J, Li Z, Cole MT, Wang A, Guo X, Liu X, et al. Nanocone-shaped carbon nanotubes field-emitter array fabricated by Laser Ablation. Nanomaterials. 2021; 11: 3244.
32. Rong Y, Cao Y, Guo N, Li Y, Jia W, Jia D. A simple method to synthesize V_2O_5 nanostructures with controllable morphology for high performance Li-ion batteries. Electrochim Acta. 2016; 222: 1691-1699.
33. Yodsin N, Sakagami H, Udagawa T, Ishimoto T, Jungsuttiwong S, Tachikawa M. Metal-doped carbon nanocones as highly efficient catalysts for hydrogen storage: Nuclear quantum effect on hydrogen spillover mechanism. Mol Catal. 2021; 504: 111486.
34. Taha HO, El Mahdy AM, El Shemy FE, Hassan MM. Hydrogen storage in SiC, GeC, and SnC nanocones functionalized with nickel, density functional theory-study. Int J Quantum Chem. 2023; 123: e27023.
35. Wei T, Zhou Y, Sun C, Guo X, Xu S, Chen D, et al. An intermittent lithium deposition model based on CuMn-bimetallic MOF derivatives for composite lithium anode with ultrahigh areal capacity and current densities. Nano Res. 2024; 17: 2763-2769.
36. Cardella U, Decker L, Sundberg J, Klein H. Process optimization for large-scale hydrogen liquefaction. Int J Hydrogen Energy. 2017; 42: 12339-12354.
37. Hammad A, Dincer I. Analysis and assessment of an advanced hydrogen liquefaction system. Int J Hydrogen Energy. 2018; 43: 1139-1151.
38. Cardella U, Decker L, Klein H. Economically viable large-scale hydrogen liquefaction. IOP Conf Ser Mater Sci Eng. 2017; 171: 012013.
39. Qyyum MA, Chaniago YD, Ali W, Saulat H, Lee M. Membrane-assisted removal of hydrogen and nitrogen from synthetic natural gas for energy-efficient liquefaction. Energies. 2020; 13: 5023.
40. Piñero JJ, Ramírez PJ, Bromley ST, Illas F, Viñes F, Rodriguez JA. Diversity of adsorbed hydrogen on the TiC (001) surface at high coverages. J Phys Chem C. 2018; 122: 28013-28020.
41. Yu X, Zhang X, Wang H, Wang Z, Feng G. High-coverage H_2 adsorption on the reconstructed Cu_2O (111) surface. J Phys Chem C. 2017; 121: 22081-22091.
42. Chettri B, Patra PK, Srivastava S, Lalhriatzuala, Zadeng L, Rai DP. Electronic properties of hydrogenated hexagonal boron nitride (h-BN): DFT study. Senhri J Multi Stud. 2019; 4: 72-79.
43. Rivard E, Trudeau M, Zaghib K. Hydrogen storage for mobility: A review. Materials. 2019; 12: 1973.

44. Thupsuri S, Tabtimsai C, Ruangpornvisuti V, Wanno B. A study of the transition metal doped boron nitride nanosheets as promising candidates for hydrogen and formaldehyde adsorptions. Physica E Low Dimens Syst Nanostruct. 2021; 134: 114859.
45. Mollaamin F, Monajjemi M. Nanomaterials for sustainable energy in hydrogen-fuel cell: Functionalization and characterization of carbon nano-semiconductors with silicon, germanium, tin or lead through density functional theory study. Russ J Phys Chem B. 2024; 18: 607-623.
46. Mollaamin F, Shahriari S, Monajjemi M. Influence of transition metals for emergence of energy storage in fuel cells through hydrogen adsorption on the MgAl surface. Russ J Phys Chem B. 2024; 18: 398-418.
47. Mollaamin F. Competitive intracellular hydrogen-nanocarrier among aluminum, carbon, or silicon implantation: A novel technology of eco-friendly energy storage using research density functional theory. Russ J Phys Chem B. 2024; 18: 805-820.
48. Mollaamin F, Monajjemi M. The influence of Sc, V, Cr, Co, Cu, Zn as ferromagnetic semiconductors implanted on B_5N_{10}-nanocarrier for enhancing of NO sensing: An environmental eco-friendly investigation. Comput Theor Chem. 2024; 1237: 114666.
49. Mollaamin F, Monajjemi M. Selectivity and sensitivity evaluation of embedded BN-nanostructure as a gas detector for air pollution scavenging: A theoretical study. Russ J Phys Chem B. 2024; 18: 1177-1198.
50. Perdew JP, Burke K, Ernzerhof M. Generalized gradient approximation made simple. Phys Rev Lett. 1996; 77: 3865.
51. Mollaamin F, Monajjemi M. Effect of implanted titanium, vanadium or chromium on boron nitride surface for increasing carbon monoxide adsorption: Designing gas sensor for green chemistry future. Russ J Phys Chem B. 2024; 18: 1199-1216.
52. Arrigoni M, Madsen GK. Comparing the performance of LDA and GGA functionals in predicting the lattice thermal conductivity of III-V semiconductor materials in the zincblende structure: The cases of AlAs and BAs. Comput Mater Sci. 2019; 156: 354-360.
53. Mollaamin F, Monajjemi M. Harmonic linear combination and normal mode analysis of semiconductor nanotubes vibrations. J Comput Theor Nanosci. 2015; 12: 1030-1039.
54. Kohn W, Sham LJ. Self-consistent equations including exchange and correlation effects. Phys Rev. 1965; 140: A1133-A1138.
55. Becke AD. Density-functional thermochemistry. III. The role of exact exchange. J Chem Phys. 1993; 98: 5648-5652.
56. Lee C, Yang W, Parr RG. Development of the Colle-Salvetti correlation-energy formula into a functional of the electron density. Phys Rev B. 1988; 37: 785-789.
57. Mollaamin F, Monajjemi M. Tailoring and functionalizing the graphitic-like GaN and GaP nanostructures as selective sensors for NO, NO_2, and NH_3 adsorbing: A DFT study. J Mol Model. 2023; 29: 170.
58. Mollaamin F, Monajjemi M. Transition metal (X = Mn, Fe, Co, Ni, Cu, Zn)-doped graphene as gas sensor for CO_2 and NO_2 detection: A molecular modeling framework by DFT perspective. J Mol Model. 2023; 29: 119.
59. Mollaamin F, Monajjemi M. In silico-DFT investigation of nanocluster alloys of Al-(Mg, Ge, Sn) coated by nitrogen heterocyclic carbenes as corrosion inhibitors. J Clust Sci. 2023; 34: 2901-2918.

60. Mollaamin F, Monajjemi M. Adsorption ability of Ga_5N_{10} nanomaterial for removing metal ions contamination from drinking water by DFT. Int J Quantum Chem. 2024; 124: e27348.
61. Mollaamin F, Monajjemi M. Molecular modelling framework of metal-organic clusters for conserving surfaces: Langmuir sorption through the TD-DFT/ONIOM approach. Mol Simul. 2023; 49: 365-376.
62. Mollaamin F, Shahriari S, Monajjemi M, Khalaj Z. Nanocluster of aluminum lattice via organic inhibitors coating: A study of freundlich adsorption. J Clust Sci. 2023; 34: 1547-1562.
63. Frisch MJ, Trucks GW, Schlegel HB, Scuseria GE, Robb MA, Cheeseman JR, et al. Gaussian 16, Revision C.01. Wallingford, CT: Gaussian, Inc.; 2016.
64. Dennington R, Keith TA, Millam JM. Gauss View, Version 6.1. Shawnee Mission, KS: Semichem Inc.; 2016.
65. Xu Z, Qin C, Yu Y, Jiang G, Zhao L. First-principles study of adsorption, dissociation, and diffusion of hydrogen on α-U (110) surface. AIP Adv. 2024; 14: 055114.
66. Schmider HL, Becke AD. Chemical content of the kinetic energy density. J Mol Struct Theochem. 2000; 527: 51-61.
67. Becke AD, Edgecombe KE. A simple measure of electron localization in atomic and molecular systems. J Chem Phys. 1990; 92: 5397-5403.
68. Tsirelson VG, Stash A. Analyzing experimental electron density with the localized-orbital locator. Acta Crystallogr B. 2002; 58: 780-785.